Solar hybrid road: from concept to modeling and lab scale mock-up experiments

Nicolas Le Touz, Jean Dumoulin, Jean Michel Piau

Solar hybrid road: from concept to modeling and lab scale mock-up experiments

N. Le Touz[a,c]*, J. Dumoulin[a,c], J-M. Piau[b]

[a]*IFSTTAR, COSYS-SII, Route de Bouaye, F-44344, Bouguenais, France*
[b]*ISFTTAR, MAST-LAMES, Route de Bouaye, F-44344, Bouguenais, France*
[c]*Inria, I4S Team, Campus de Beaulieu, F-35042 Rennes, France*

Abstract

We present in this paper the concept of solar hybrid road and the numerical model studied and develop to compute its thermal state at any time step. The aim of these new structures is to collect part of the solar radiation during the summer period, to prevent from icing at the surface during the winter period. As it is reversible, it will help also to prevent from a too high structure temperature (in particular closed to the surface) in summer season. Two types of modifications, compared to traditional structures are presented. The first one concerns the insertion of a porous layer allowing a heat fluid to exchange thermal energy. The second one concerns the use of a semi-transparent material at pavement surface allowing the solar radiation to penetrate deeper in the structure. The numerical model of this multi-physics problem develop with the finite element method is presented and discussed. A validation on two test cases is proposed. First results on energy harvesting evaluation for few locations (*i.e.* climatic conditions) in France are presented and discussed. Finally, conclusion and perspectives are proposed.

Keywords: Solar hybrid road; multi-physics; finite element method; thermal heat transfer; energetic system.

* Corresponding author. Tel.: +33 (0)2 40 84 59 02; fax: +33 (0)2 40 84 59 98.
E-mail address: nicolas.le-touz@ifsttar.fr

Nomenclature

C_p	volumic thermal capacity	Op	opaque
k	thermal conductivity	κ	monochromatic absorption coefficient
$\vec{u}$	fluid velocity	φ	porosity
T	temperature	ρ	density
I_ν	monochromatic intensity	ρ_ν	monochromatic reflection coefficient
ϵ_ν	monochromatic emissivity	σ	Stefan constant
ST	semi transparent	σ_ν	monochromatic scattering coefficient

1. Introduction

Car traffic on roads represents at the same time economic, safety and ecologic stakes, which are particularly important during extreme environmental conditions, as heat waves or cold spells. In particular, winter conditions can entail black ice occurrence and/or snow accumulation on roads, increasing the risk of car crash and reducing the economic activities. The solution of pouring salt on roads submitted to such environmental conditions allows to maintain traffic, but have the drawback to be expensive. In fact, in North America, about 14 million tons of salt are used annually (Transportation Research Board (1991)). In France, this quantity reaches 1 million tons (Parienté (2011)). Because of the cost of salt, which is about 100 € per ton, from Schepman (2010), using salt for deicing has a non-negligible economic impact for the society, in addition to the ecological impact on the fauna and the flora, according to Sanzo and Hecnar (2006), due to flow of brine to rivers and ground water. This ecological impact can be evaluated to 450 M€ in Germany according to Huckestein and Verron (1996). Salt increases also corrosion on bridges, what entails a decrease in the lifetime of the structure (Stewart (1998)).
In order to avoid these disagreements, there is also an interest to investigate alternative solutions to deice roads. One of these solutions is to heat the surface of the road (The Hybrid Solar Road (2015)). Different methods exist to heat the pavement: some electrical resistance can be buried in the pavement. Oil- or gas based road heating system can also be brought into play (Eugster (2007)). However, heating roads need a large amount of energy. This high consumption can represent, for 20 square meters of pavement, the annual consumption in energy for hot water of a family (Chen et al. (2011)).
Due to amount of energy required for de-icing and cost consideration, alternative solutions have been studied and developed, in particular ones based on geothermal approaches. Such solution allows to use the energy stored in the ground during the summer when freezing conditions occur. It has moreover the advantage of needing less maintenance (Chen (2011)). For the main part of these systems, the heat fluid flows in tubes buried below the pavement. We propose here a solution with a fluid flowing in a porous layer below the surface layer. To increase the ability of this hybrid road to store energy, a semi-transparent layer is used in order that the solar radiation can penetrate deeply inside the structure.
In this paper, we present a numerical model developed and studied to calculate evolution of the temperature field in the structure under known environmental conditions. It is used to establish annual energy recovery performances of these hybrid roads for various climatic conditions. In our numerical model three physical phenomena have been integrated: thermal diffusion in the whole structure, hydraulic convection in the porous layer and radiative heat transfer in the semi-transparent layer. Numerical resolution of this multi-physic problem is performed with the finite element method. We first introduce the concept of hybrid solar road, then the numerical model developed for each physic, then we detail the numerical coupling and present a comparison with measured data obtained on a laboratory mock-up. Finally, we present and discuss first results obtained on energetic performances.

2. Hybrid solar road concept

We focus here on the study of a multilayer system for which the two layers closest to the surface of the road are modified, compared to traditional road structures

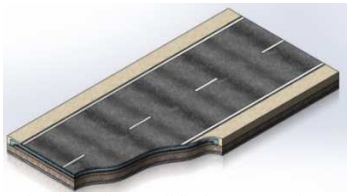

Figure 1: Schematic view of a modified structure from a 3D CAD

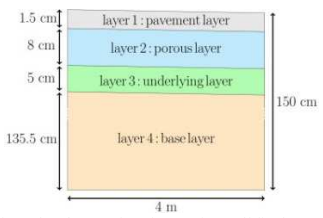

Figure 2: Sectional schematic view of modified road structure

Figure 2 represents a sectional view of the studied pavement. Layer 1 is opaque or semi-transparent and waterproof. Layer 2 is porous: a fluid flows inside along the width of the road, with the effect of the imposed slope. Layer 3 and 4 are opaque and waterproof.
This fluid flow allows to collect a part of solar radiation during summer period. On the contrary, under winter conditions, it allows to heat the surface of the pavement and also to prevent from icing (Asfour (2016)).
The structure is also submitted to three coupled thermal phenomenon: heat diffusion and radiative transfer in the semi-transparent layer, heat diffusion and hydraulic convection in the porous layer and heat diffusion anywhere else. Numerical model of these three physical phenomena and their coupling are detailed in the next section.
For numerical computation, the studied structure has a length equal to 4 m, a height equal to 1.5 m. To reduce computation time, the structure is considered in 2 dimensions when conducting numerical simulations over a year. Thermal properties considered for the pavement layers are reported in table 1.

Table 1. Thermal properties of the layers of the structure and fluid, from Asfour et al. (2016), Incropera and DeWitt (1990) and Taine et al. (2014)

	Layer 1	Layer 2	Layer 3	Layer 4	Fluid
k [W.m^{-1}.K^{-1}]	0.85	1.03	1.40	1.10	0.60
ρ [kg.m^{-3}]	2700	2360	2620	2300	1000
C_p [J.kg^{-1}.K^{-1}]	840	780	860	1000	4180

Optical properties for the semi-transparent material vary with considered wavelength. For calculus, we use absorption coefficient given by Ping and Lallemand (1989) along each spectral band. These values are reported in table 2. Semi-transparent pavement is a diffusive medium; we take a scattering coefficient equal to 10 m^{-1}.

Table 2. Optical properties of the semi-transparent media

λ [µm]	$\lambda < 0.5$	$0.5 \leq \lambda < 2.7$	$2.7 \leq \lambda < 4.5$	$4.5 \leq \lambda < 50$	$\lambda \geq 50$
κ_λ [m^{-1}]	0	10	1000	5000	$+\infty$
σ_λ [m^{-1}]	10	10	10	10	10

3. Multi-physic numerical model studied and developed

Our model combined three Physics using Finite Element Modelling approach and is presented hereafter.

3.1. Thermal diffusion

Thermal diffusion occurs in the whole structure. We consider here that the surface of the structure is submitted to convective exchanges with the ambient air, radiative exchanges with the atmosphere and solar radiation. Moreover, we suppose that there is no precipitation and no water nor snow at the surface. Other boundaries are supposed to be adiabatic. In particular, the depth of the considered domain is supposed to be large enough so that thermal exchange at its opposite boundary can be neglected. Heat diffusion equation to solve is reported in system (1)

$$\begin{cases} \rho C_p \dfrac{\partial T}{\partial t} = \nabla \cdot [k \nabla T] + q \text{ on } \Omega \\ k \nabla T \cdot \vec{n} = \Phi_s + h(T_a - T) + \varepsilon\sigma(T_c^4 - T^4) \text{ on the surface} \\ k \nabla T \cdot \vec{n} = 0 \text{ on the other boundaries} \end{cases} \quad (1)$$

Modelization of thermal diffusion with the finite element method is well-documented, for instance in Gartling and Reddy (2010) or Taine et al. (2014).

3.2. Hydraulic convection

The porous layer, with a porosity written φ, is supposed to be fully saturated in fluid. Fluid flow can be described by the Darcy law: the fluid velocity $\vec{u}$ is written as equation (2):

$$\vec{u} = \frac{-K\rho g}{\mu} \nabla \left(\frac{p}{\rho g} + z \right) \quad (2)$$

Where K is the permeability (in m^2), g is the acceleration of gravity and μ the dynamic viscosity (in Pa.s).
Two temperature fields are studied: a temperature field for the solid phase, noted T, defined in the whole domain Ω, and a temperature field for the fluid phase T_f, only defined on the porous domain Ω_f.
Heat equation is formulated at a microscopic scale, then the use of a representative elementary volume allows to get a coupled system of equation involving mean values, on each representative elementary volume, involving both temperature fields. The system of equations is written, from Bejan et al. (2004), or Nield and Bejan (2013):

$$(1-\varphi)\rho C_p \frac{\partial T}{\partial t} = (1-\varphi)\nabla \cdot [k\nabla T] + h_{fs}a_{fs}(T_f - T) \tag{3}$$

$$\varphi\rho_f C_{pf} \frac{\partial T_f}{\partial t} + \rho_f C_{pf}\vec{u} \cdot \nabla T_f = \varphi\nabla \cdot [k_f \nabla T_f] + h_{fs}a_{fs}(T - T_f) \tag{4}$$

Where the index f refers to the fluid phase, no index refers to the solid phase and $h_{fs}$is an exchange coefficient given by (5), from Nield and Bejan (2013):

$$\frac{1}{h_{fs}} = \frac{d_p}{Nu_{fs}k_f} + \frac{d_p}{\beta k} \tag{5}$$

a_{fs} is the specific surface (surface by volume unit), given by $a_{fs} = \frac{6(1-\varphi)}{d_p}$, d_p is the aggregate size, Nu_{fs} the Nüsselt number and β a constant.
For the solid phase, boundary conditions are those described in (1). Moreover, for internal boundaries, the temperature field is supposed to be known. Two external boundaries are considered: with the fluid input and with the fluid output. The solid phase is supposed to be submitted to a Neumann boundary condition at the input, denoted by Γ_{f0}: $k\nabla T \cdot \vec{n} = h_f(T_{f0} - T)$, with T_{f0} the input fluid temperature. At the output, we suppose an adiabatic boundary condition, as also used by Asfour et al. (2016).
By written (ϕ_i) a basis of $L^2(\Omega_f)$, temperature fields can be written $T = \sum_i \phi_i T_i$ and $T_f = \sum_i \phi_i T_{f,i}$. Because of the advection term $\rho_f C_{pf}\vec{u} \cdot \nabla T$, the equation (4) is hyperbolic, so solving numerically this equation with finite element method can entail spurious oscillations on the numeric solution (Johnson (1987). Meinköhn (2009)). A Petrov-Galerkin formulation, which was detailed by Brooks and Hughes (1982) and Johnson (1987) allows to prevent from these non-physical oscillations by adding an upwind term $\vec{u} \cdot \nabla\phi_i$ to the test function ϕ_i. The choice of the damping parameter δ is mainly due to the mesh size. Discussion about this parameter is proposed in Brooks and Hughes (1982), Codina (1998), Donea and Huerta (2003), and Shakib et al. (1991).
For any ϕ_j, the Petrov-Galerkin formulation give us the equations (6) and (7):

$$\begin{aligned}\sum_i \left\{(1-\varphi)\left(\int_{\Omega_f} \rho C_p \phi_i \phi_j \mathrm{d}\Omega\right)\frac{\partial T_i}{\partial t} + (1-\varphi)\left(\int_{\Omega_f} \nabla\phi_i k \nabla\phi_j \mathrm{d}\Omega + \int_{\Gamma_{f0}} h_f \phi_i \phi_j \mathrm{d}\Gamma\right) T_i\right\} \\ = \left(\int_{\Gamma_{f0}} h_f \phi_j T_{f0} \mathrm{d}\Gamma\right) + \sum_i \left\{\left(\int_{\Gamma_f} h_{fs} a_{fs} \phi_i \phi_j \mathrm{d}\Gamma\right)(T_{f,i} - T_i)\right\}, \forall j\end{aligned} \tag{6}$$

$$\begin{aligned}\sum_i \left\{\varphi\left(\int_{\Omega_f} \rho_f C_{pf} \phi_i (\phi_j + \delta\vec{u} \cdot \nabla\phi_j)\mathrm{d}\Omega\right)\frac{\partial T_{f,i}}{\partial t}\right. \\ \left. + \left(\varphi\int_{\Omega_f} \nabla\phi_i k \nabla\phi_j \mathrm{d}\Omega + \int_{\Omega_f} (\phi_j + \delta\vec{u} \cdot \nabla\phi_j)\rho_f C_{pf}\vec{u} \cdot \nabla\phi_i \mathrm{d}\Omega\right) T_{f,i}\right\} \\ = \sum_i \left\{\left(\int_{\Omega_f} h_{fs} a_{fs} \phi_i (\phi_j + \delta\vec{u} \cdot \nabla\phi_j)\mathrm{d}\Omega\right)(T_i - T_{f,i})\right\}, \forall j\end{aligned} \tag{7}$$

3.3. Radiative transfer in the semi-transparent layer

We present in this part the modeling of thermal diffusion and radiative transfer coupling effects for the semi-transparent layer. This one is transparent for solar radiation, and opaque for high wavelength radiation. The aim of this section is to compute the intensity of radiation in the semi-transparent layer in order to get the thermal source. Radiative transfer in the layer can be quantified by computing the radiative intensity I_ν, which is governed by the radiative transfer equation introduced by Chandrasekhar (1960):

$$\vartheta \cdot \nabla I_\nu(x,\vartheta) = -(\kappa_\nu + \sigma_\nu) I_\nu(x,\vartheta) + \kappa_\nu B_\nu(T(x)) + \frac{\sigma_\nu}{4\pi}\int_{4\pi} p_\nu(\tilde{\vartheta},\vartheta) I_\nu(x,\tilde{\vartheta})\mathrm{d}\tilde{\vartheta} \tag{8}$$

Where x denotes the position ($x \in \Omega$), ϑ refers to the direction ($\vartheta \in S^2$, the unit sphere). The transitional term is neglected, the evolution of phenomenon being slow (Howell and Siegel (2010)).
Radiative transfer equation is defined both in position along x and in direction along ϑ. The domain, here $\Omega \times S^2$, is also in five dimensions. The boundaries need to be divided into two parts: input boundary Γ^- and output boundary Γ^+, which are defined as:

$$\Gamma^+ = \{(x,\vartheta) \in \partial\Omega \times S^2 \text{ such as } \vec{n}\cdot\vartheta \geq 0\} \quad (9)$$
$$\Gamma^- = \{(x,\vartheta) \in \partial\Omega \times S^2 \text{ such as } \vec{n}\cdot\vartheta < 0\} \quad (10)$$

These boundaries are shown, for a given direction ϑ, in Figure 3.

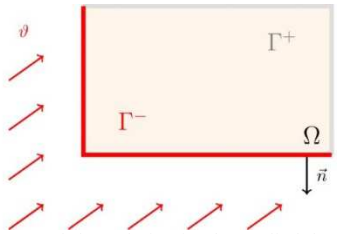

Figure 3: Sub-boundaries for the studied domain

Boundary conditions are required only in the input boundaries, due to the structure of the radiative transfer equation. Radiative intensity at the input boundaries comes from external sources such as solar radiation and internal contributions due to reflections:

$$I_\nu(x,\vartheta) = g_{out}(x,\vartheta) + g_{in}(x,\vartheta,I_\nu), \text{ for } (x,\vartheta) \in \Gamma^- \quad (11)$$

Some methods in literature allows to solve the radiative transfer equation, as finite volume, Monte Carlo, spherical harmonics (Howell and Siegel (2010), Modest (2003)). We propose here to focus on the finite element method presented by Kanschat (2009) and Richling (2001) for radiative transfer applied in astrophysics. The finite element method is here transposed and adapted for the case of a semi-transparent solid media with small dimensions.
Two discretization are required for directional and spatial dependences. Directional discretization is performed with the discrete ordinate method. For a directional mesh, based on the unit sphere, with N_S nodes ϑ_i located at the center of elements of weight w_i, integral terms on directions can be approximated, for any variable u continuous along the unit sphere, by the expression in equation (12):

$$\int_{4\pi} u(\vartheta)\, d\vartheta = \sum_{i=1}^{N_S} w_i u(\vartheta_i) \quad (12)$$

This discretization is equivalent to a discontinuous Galerkin method with constant interpolation functions on the elements. In order to get a mesh with the most uniform allocation of direction nodes, we propose to use a mesh based on a regular polyhedron with triangular faces, as the icosahedron suggested by Richling et al. (2001). Each direction of the mesh linked the center of the unit polyhedral to the centroid of a face. Weights being equal to the projected area of the face on the unit sphere, all weights are equal to $\frac{4\pi}{N_S}$. The number of directions can be increased recursively by divided each triangular face into four similar triangles, this number of directions being also multiplied by four at each iteration.
Applying the discrete ordinate method to the equations (11) and (12) allows to obtain the system (13) and the boundary conditions (14). (13) and (14) are systems of N_S equations, defined only on space:

$$\vartheta_k \cdot \nabla I_\nu(x,\vartheta_k) = -(\kappa_\nu + \sigma_\nu) I_\nu(x,\vartheta_k) + \kappa_\nu B_\nu\big(T(x)\big) + \frac{\sigma_\nu}{4\pi}\sum_{l=1}^{N_S} w_i p_\nu(\vartheta_l,\vartheta_k) I_\nu(x,\vartheta_l)\,, \quad \forall (x,k) \in \Omega \times [|1,N_S|] \quad (13)$$

$$I_\nu(x,\vartheta_k) = g_{out}(x,\vartheta_k) + g_{in}(x,\vartheta_k,I_\nu)\,, \forall (x,\vartheta_k) \in \Gamma^- \quad (14)$$

To apply the finite element method on this coupled system of equations, we introduce the following notations:

- $W_\Omega = \{u \in L^2(\Omega) \text{ such as } \forall \vartheta \in S^2, \vartheta \cdot \nabla u \in L^2(\Omega \times S^2)\}$
- $\partial\Omega_k^- = \{x \in \partial\Omega \text{ such as } \vec{n}(x)\cdot\vartheta_k < 0\}$

- $W_{0,k} = \{u \in L^2(\partial\Omega_k^-)\}$

We define inner products $\langle\cdot,\cdot\rangle_\Omega$ on Ω and $\langle\cdot,\cdot\rangle_{k^-}$ on $\partial\Omega_k^-$ such as:

$$\langle u, v\rangle_\Omega = \int_\Omega u(x)v(x)d\Omega \ , u, v \in W_\Omega \tag{15}$$

$$\langle u, v\rangle_{k^-} = \int_{\partial\Omega_k^-} u(x)v(x)dS \ , u, v \in W_{0,k} \tag{16}$$

The systems of equations (13) and (14) can also be rewritten under weak form with these notations, under a basis (φ_i) of $L^2(\Omega)$:

$$\langle \mathcal{A}_\nu I_\nu(\cdot, \vartheta_k), \varphi_i\rangle_\Omega = \langle f_k, \varphi_i\rangle_\Omega \tag{17}$$

$$\langle \mathcal{B}_\nu I_\nu(\cdot, \vartheta_k), \varphi_i\rangle_{k^-} = 0 \tag{18}$$

With $\mathcal{A}_\nu$ and $\mathcal{B}_\nu$ two linear operators.

As for the hydraulic convection equation (4), radiative transfer equations discretized in directions (13) are hyperbolic if there is scattering in the media. To avoid spurious oscillations, a regularization needs to be applied. We overcome this problem with a Petrov-Galerkin formulation. Moreover, we inject boundary conditions (18) as weak constraints in the system (17). The systems (17) and (18) are then rewritten as:

$$\langle \mathcal{A}_\nu I_\nu(\cdot, \vartheta_k), \varphi_i + \delta\vartheta_k \cdot \nabla\varphi_i\rangle_\Omega + \langle \mathcal{B}_\nu I_\nu(\cdot, \vartheta_k), \varphi_i\rangle_{k^-} = \langle f_k, \varphi_i\rangle_\Omega \ , \forall k \in [|1, N_S|] \tag{19}$$

For a spatial mesh with N_Ω nodes, we get a linear system with $N_\Omega \times N_S$ unknowns for each frequency interval.

Absorption of radiation and heat production in the semi-transparent media occur by two ways. In the material itself, absorption of radiation entail a volumic heat source denoted here by S_{vol}, and at boundaries between semi-transparent and opaque media, there is also absorption of radiation which can be written under the form of a heat flux S_{flux}. Both two components can be written as equations (20) and (21) as suggest by from Modest (2003).

$$S_{vol} = -\nabla \cdot \left[\int_{\nu=0}^{+\infty}\int_{4\pi} I_\nu(x, \vartheta)\vartheta d\vartheta d\nu\right] \tag{20}$$

$$S_{flux} = \int_{\nu=0}^{+\infty}\left[(1-\rho_\nu)\int_{\vartheta\cdot\vec{n}>0} I_\nu(x, \tilde{\vartheta})\,\tilde{\vartheta}\cdot\vec{n}d\vartheta - \epsilon_\nu\pi B_\nu(T(x))\right]d\nu \tag{21}$$

3.4. Solving the coupled problems : Thermal diffusion, Hydraulic convection and Radiative transfer

Temperature field in the structure is computed dynamically from environmental data (sky temperature, air temperature and solar radiation). At each temporal iteration, radiative transfer equation is first solved (system (19) discretized in space), allowing to get the intensity field, then source terms are computed with (20) and (21). The heat sources terms are then injected in the heat diffusion equation (1), which is coupled with the hydraulic convection equations (6) and (7). A Crank-Nicholson scheme is used for the temporal resolution.

4. Validation of the numerical model

Two test cases are presented hereafter.

4.1. Solar road with opaque surface in established steady state

We focus in this section on the case of an opaque surface layer, for an established steady state. The aim is here to get an estimation of the minimal input temperature of the fluid allowing to maintain the surface temperature higher than 0°C. Two methods are used: the numerical model presented in previous sections and an analytical formulation. This formulation is first described. The studied road structure is presented in figure 5 (left).

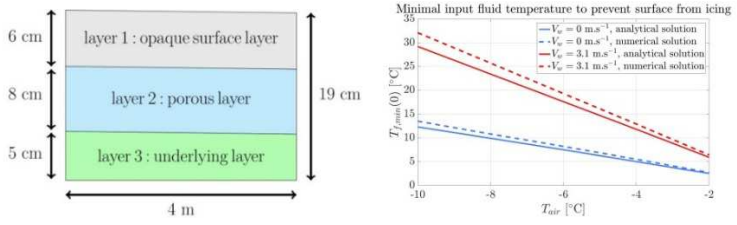

Figure 5: Studied structure for established steady state (left image) - Minimal fluid temperature to prevent surface from icing as a function of air temperature (right graph)

We consider in this paragraph a one dimension problem: temperature in layers depends only from the distance to the injection point. Three layers are supposed to constitute the road structure: the porous layer is located between two impermeable layers.
We suppose moreover that temperature in the middle of layers is equal to the mean temperature between the extremities of the layer and that there is a local thermal equilibrium. Under these assumptions, it can be shown that the temperature of the fluid can be written as an explicit function of the distance s to the injection point:

$$T_f(s) = T_f(0)e^{-\frac{s}{\kappa}} + T_\infty\left(1 - e^{-\frac{s}{\kappa}}\right) \tag{22}$$

With :

- $T_\infty = \frac{h_{conv}T_{air} + r_{rad}T_{sky} + \Phi}{h_{conv} + h_{rad}}$,
- $\kappa = \frac{\rho_f c_f h_{dr} u(r_{ps} + h_{conv} + h_{rad})}{r_{ps}(h_{conv} + h_{rad})}$,
- $r_{ps} = \frac{2k_s k_p}{h_s k_p + h_p k_s}$.
- Φ refers to the solar radiation,
- T_{air} to the air temperature,
- T_{sky} to the sky temperature,
- h_s to the thickness of the surface layer,
- h_p to the thickness of the porous layer,
- k_s to the thermal conductivity of the surface layer,
- k_p to the thermal conductivity of the porous layer,
- u to the Darcy velocity of the fluid,
- h_{conv} to the convective exchange coefficient
- h_{rad} to the radiative exchange coefficient.

The temperature of the surface layer T_s can then be written as:

$$T_s(s) = \frac{r_{drs}T_f(s) + h_{conv}T_{air} + h_{rad}T_{sky} + \Phi}{r_{ps} + h_{conv} + h_{rad}} \tag{23}$$

By denoting L the width of the road, the input temperature of the fluid allowing to maintain a surface temperature higher than 0°C can be calculated:

$$T_{f,min}(0) = -e^{\frac{L}{\kappa}}\left(\frac{1}{r_{ps}}\left(h_{conv}T_{air} + h_{rad}T_{sky} + \Phi\right) + T_\infty\left(1 - e^{-\frac{L}{\kappa}}\right)\right) \tag{24}$$

In a first approach, we consider here that solar road structure is studied under constant environmental conditions, what can be performed with a climatic chamber. We suppose although that the sky temperature is equal to the air temperature and that there is no solar radiation. Under these assumptions, equation (24) can be rewritten:

$$T_{f,min}(0) = -e^{\frac{L}{\kappa}}\left(\frac{h_{conv} + h_{rad}}{r_{ps}} + 1 - e^{-\frac{L}{\kappa}}\right)T_{air} \tag{25}$$

A Darcy velocity value equal to 2.18×10^{-4}m.s^{-1}, corresponding to a slope of 1% and a permeability of 2.18×10^{-2}m.s^{-1} (Asfour (2016)), is chosen. We consider the structure presented in figure 5 and the thermal parameters of table 1. Two wind speed are studied: $V_w = 0$ *m.s*$^{-1}$ and $V_w = 3.1$ *m.s*$^{-1}$, with a convective exchange coefficient given by $h_{conv} = 5.6 + 4V_w$, also used by (Asfour (2016)). Results for input fluid temperature both with (25) and numerical simulation are given in table 3.

Table 3. Minimal temperature (in °C) for input fluid allowing to maintain a positive temperature along the surface

Wind speed	Method	$T_{air} = -10$°C	$T_{air} = -8$°C	$T_{air} = -6$°C	$T_{air} = -4$°C	$T_{air} = -2$°C
0	analytic	12.3	9.9	7.5	5.0	2.5
0	our model	13.5	10.8	8.2	5.5	2.7
3.1	analytic	29.2	23.4	17.6	11.8	5.9
3.1	our model	32.1	25.7	19.3	12.9	6.4

The comparison between analytic and numerical formulation is shown in figure 5 (right). The input temperature with the analytic formulation is close to the computed solution, with a difference of about 10%. It can be noticed that the analytical formulation always under evaluates the input temperature compared to the computed

temperature. Such difference may be explain by the thermal diffusion in the second dimension that is not considered. There is no temperature variation in surface layer along the depth, so the surface temperature corresponds more to the temperature at the middle of the surface layer rather than the temperature at its the surface, which is lower.

4.2. Solar road with semi-transparent surface: comparison with data acquired on a laboratory mock-up

In order to study the validity of our approach for the semi-transparent surface layer, a mock-up has been built (figure 6). A 1500 W halogen lamp at 3000 K allows to simulate the solar heat flux and the input fluid temperature is measured with a thermocouple. A FLIR A65 infrared camera allows to measure the surface temperature of the structure. A meteorological station and a pyranometer measure the relative humidity, ambient temperature and the solar radiation flux density.

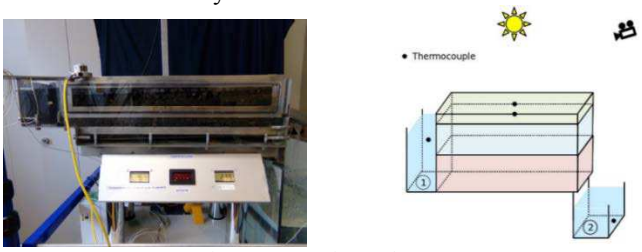

Figure 6: Experimental set-up

An example of thermal image obtained with the infrared camera is presented in figure 7.

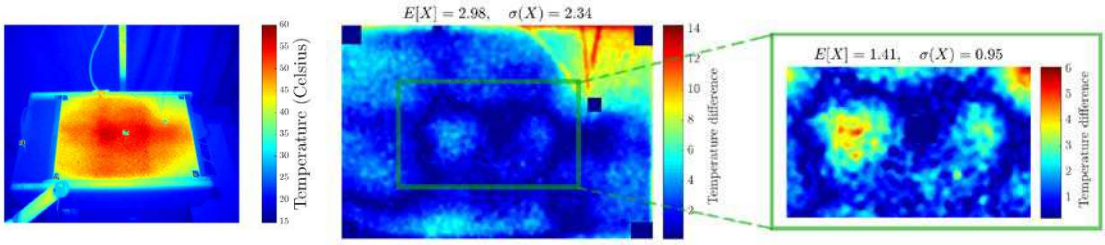

Figure 7: Example of infrared image captured by the infrared camera (left image) - Comparison of measured temperature with the numerical simulation (middle image with zoom on right)

The halogen lamp is switched on during some hours, allowing to get a permanent established regime. Knowledge of environmental conditions enables us to apply the numerical model presented in section 2. A comparison between numerical and experimental data can then be led. The difference of surface temperature between the numerical model and measurements from the infrared camera is presented in figure 7 (right). On a central area, the difference of temperature between experiments and numerical simulations is about 1 °C. The numerical model drives to results close to the measures. Photovoltaic panels being present in the mock-up can explain a part of the observed temperature difference.

5. Energy harvesting performance evaluation: preliminary results and analysis

In this section, we determine the energetic performance of solar hybrid roads for energy harvesting over a year and for few climatic conditions in France. Annual weather data are used for eight locations in France, corresponding to the main climatic conditions.

The schematic sectional view of the structure was shown in figure 2. The fluid is injected in the porous layer at a constant temperature, equal to 15°C in the presented numerical simulations. Environmental conditions entail temporal variations of the temperature field in the structure and also for the temperature of the fluid at the output of the structure. The velocity of the fluid flow is supposed to be maintained constant, equal to 1×10^{-4}m.s^{-1}. Thermal and optical properties are supposed to be independent from temperature and from mechanical evolution of the structure over time.

We consider here only the ability of the structure to recover energy, that is to say that we consider only the moments when the output temperature of the fluid is higher than the input temperature. This variation of temperature between the input and the output is supposed to allow energy recovering when positive.

Simulations are performed on more than one year of data, so that initial conditions are erased. Since output temperature during winter period is most of the time lower than the input temperature, only summer period is considered for energy recovering, from May to October.

Energy recovering capacity is defined as:

$$E = \int_t \rho_f C_{p,f} h_{Po} u (T_{sortie} - T_{entree})^+ dt \quad (22)$$

With $(\cdot)^+$ referring to the positive part and h_{Po} to the thickness of the porous layer.
The eight locations studied are submitted to various solar radiation conditions during this period, with cumulated solar contributions between 4047 kWh.m^{-2} in Nancy and 5524 kWh.m^{-2} in Carpentras, as shown in figure 8 (left).

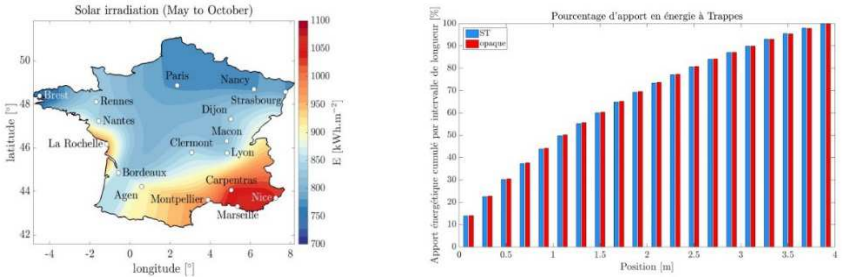

Figure 8: Cumulated solar radiation (May-October period) on left - Evolution of the part of final energy recovery along the width of the structure for opaque and semi-transparent pavements (right)

Efficiency of this modified structure can be evaluated by calculating the ratio between the energy harvested by the system and the cumulated solar radiation during the studied period. Results obtained are shown in table 3. This table also shows that the structure with a semi-transparent pavement allows to collect more energy than the one with the opaque pavement. For opaque surface wearing course, the gain is between 21 and 29% of the recoverable energy. Efficiency values presented in table 3 show that the gain of efficiency by using a semi-transparent pavement surface layer is between 6.5 and 7% of the incoming solar radiation for all these locations.

Table 3. Results for 4m width opaque and semi-transparent pavement

Location	Solar cumulated input (Op pavement)[kWh/m^2]	Recoverable energy (Op pavement) [kWh/m^2]	Efficiency (Op pavement) [%]	Recoverable energy (ST pavement) [kWh/m^2]	Efficiency (ST pavement) [%]	Energy gain [kWh/m^2]
Agen	4615	1440	31,2	1744	37,7	+304 (+21%)
Carpentras	5524	1812	32,8	2188	39,6	+376 (+21%)
La Rochelle	4973	1288	25,9	1657	33,2	+369 (+29%)
Macon	4164	1299	31,2	1581	37,8	+282 (+22%)
Nancy	4047	1117	27,6	1394	34,4	+277 (+25%)
Nice	5437	1805	33,2	2201	40,4	+396 (+22%)
Rennes	4336	1084	25,0	1386	31,9	+302 (+28%)
Trappes	4312	1190	27,6	1470	34,1	+280 (+24%)

These data of recoverable energy also depend highly from the width of the road. In fact, the efficiency of this heat exchanger decrease as the length of the flow increases. This deterioration of the performances of the structure with its width is shown in figure 8 (right). This figure represents the ratio of evolution of the energy recovery term E computed from equation (22) for some lengths from the input area on the energy recovery at the output of the structure, after 4 meters. This figure points out the fact that half of the contribution for energy recovering occurs less than 1.4 meter after the injection of the heat fluid. On the same way, 90% of the contribution occurs after about 3 meters, at 75% of the width of the structure. For dimensioning the structure, it is also important to take into account this decrease in performances, the same length yielding more energy if located near the injection area. There are however no significant differences between both pavements.

6. Conclusion

In this study, we have presented the concept of solar hybrid road. In order to get an estimation of energetic performance of such structures, multi-physics numerical model has been studied and developed, implying thermal diffusion, hydraulic convection and radiative transfer. Each physic has been described and finite element method has been applied on each of them, with variations of the Galerkin formulation for hydraulic convection

and radiative transfer equations. A numerical coupling has been then explained in order to realize numerical simulation relying on environmental data.
Our numerical model has been compared with data coming from two test cases: first, a comparison with an analytical expression in steady state has been performed with an opaque surface layer. Finally, numerical data from the model are compared with data acquired on a mock-up with a semi-transparent surface layer submitted to a radiative heat flux. These two test cases show that the numerical model is coherent with particular test case allowing analytical solution or experimental results obtained in laboratory conditions.
First results obtained for energy harvesting performances have been presented and discussed.

Future works will refine energy harvesting performance evaluation and also address heating efficiency (during winter season).

Acknowledgements

French Ministry of "Transition écologique et solidaire" for supporting part of this work under grant agreement DGITM N° 17/389.

7. References

Asfour, S., Bernardin, F., Toussaint, E. and Piau, J. M., 2016, *Hydrothermal modeling of porous pavement for its surface de-freezing*, Applied Thermal Engineering, 107: 493–500

Bejan, A., Dincer, I., Lorente, S., Miguel, A. F. and Reis, A. H., 2004, *Porous and Complex Flow Structures in Modern Technologies*, first edition, Springer-Verlag, New York

Brooks, A. N. and Hughes, T. J., 1982, *Streamline Upwing/Petrov-Galerkin formulations for convection dominated flows with particular emphasis on the incompressible Navier-Stokes Equations*, Computer Methods in Applied Mechanics and Engineering, 32:199–259

Chandrasekhar, S., 1960, *Radiative Transfer*, Dover Publications

Chen, M., Wu, S., Wang, H. and Zhang, J., 2011, *Study of ice and snow melting process on conductive asphalt solar collector*, Solar Energy Materials & Solar Cells, 95: 3241–3250

Codina, R., 1998, *Comparison of some Finite Element Methods for Solving the Diffusion-Convection-Reaction Equation*, Comput. Methods Appl. Mesh. Engrg, 156:185-210

Donea, J. and Huerta, A., 2003, *Finite Element Methods for Flow Problems*, John Wiley & Sons, Chichester

Eugster, W. J., 2007, Road and Bridge Heating Using Geothermal Energy, in *Proceedings European Geothermal Congress*, Unterhaching, Germany

Gartling, D. K. and Reddy, J. N., 2010, *The Finite Element Method in Heat transfer and Fluid Dynamics*, Third Edition, CRC Press

Incropera, F. P. and DeWitt, D. P., 1990, *Fundamentals of Heat and Mass Transfer*, third edition, Wiley

Howell, J. R. and Siegel, R. and Pinar, M. P., 2010, *Thermal Radiation Heat Transfer*, 5th edition, CRC Press

Huckestein, B. and Verron, H., 1996, *Externe Effekte des Verkehrs in Deutschland*, In: UBA-Texte 66/96; Mobilität um jeden Preis? Exportenworkshop zu den externen kosten des Verkehrs und den Möglichkeitensie zu verringern. Umweltbundesamt Berlin.

Kanschat, G., 2009, *Solution of Radiative Transfer Problems with Finite Elements*, in Numerical Methods in Multidimensional Radiative Transfer, Kanschat, G., Meinköhn, E., Rannacher, R. and Wehrse, R., eds., Springer-Verlag, Berlin

Modest, M., 2003, *Radiative Heat Transfer*, second edition, Academic Press

Nield, D. A. and Bejan, A., 2013, *Convection in Porous Media*, fourth edition, Springer

Parienté, J., 2010, Sur les routes : de la neige, de la glace… et du sel, lemonde.fr, Available on http://www.lemonde.fr/planete/article/2010/01/12/sur-les-routes-de-la-neige-de-la-glace-et-du-sel_1290877_3244.html [accessed on 2017, August 23rd]

Ping, T. H. and Lallemand, M., 1989, *Transient radiative-conductive heat transfer in flat glasses submitted to temperature, flux and mixed boundary conditions*, Int. J. Heat Mass Transfer, 32(5):795–810

Richling, S., Meinkohn, E., Kryzhevoi, N. and Kanschat, G., 2001, *Radiative Transfer with Finite Element. i. Basic Method and Tests*, A&A, 380:776–788

Sanzo, D. and Hecnar, S. J., 2006, *Effects of road de-icing salt (NaCl) on larval wood frogs (Rana sylvatica)*, Environmental Pollution, 140, 247–256

Schepman, T., 2010, Neige : combien coûte le régime de déneigement au sel ?, 20minutes.fr, Available on http://www.20minutes.fr/economie/636587-20101209-economie-neige-combien-coute-regime-deneigement-sel [accessed on 2017, August 23rd]

Shakib, F., Hughes, T. J. R. and Johan, Z., 1991, A new Finite Element Formulation for Computational Fluid Dynamics: X. The Incompressible Euler and Navier-Stokes Equations, Computer Methods in Applied Mechanics and Engineering, 89:141–219

Stewart, M. G. and Rosowsky, D. V., 1998, Time-dependant reliability of deteriorating reinforced concrete bridge decks, Structural Safety, 20:91–109

Taine, J., Enguehard, F. and Iacona, E., 2014, *Transferts thermiques, introduction aux transferts d'énergie*, fifth edition, Dunod

The Hybrid Solar Road, 2015, Press Release, Available on http://www.ifsttar.fr/fileadmin/redaction/5_ressources-en-ligne/Communication/Espace_presse/Dossiers_de_presse/Route_solaire_En.pdf [accessed on 2017, August 23rd]

Transportation Research Board, 1991, *Special Report 235: Highway Deicing Comparing Salt and Calcium Magnesium Acetate*. Committee on the Comparative Costs of Rock Salts and Calcium Magnesium Acetate (CMA) for Highway Deicing. National Research Council, Washington, DC